Fatigue strength characterization of high and ultra-high-strength steel cut edges

Lipiäinen Kalle, Ahola Antti, Skriko Tuomas, Björk Timo

DOI: 10.1016/j.engstruct.2020.111544

Fatigue strength characterization of high and ultra-high-strength steel cut edges

Kalle Lipiäinen, Antti Ahola, Tuomas Skriko & Timo Björk

Laboratory of Steel Structures, Lappeenranta-Lahti University of Technology LUT, P.O. Box 20, FI-53851 Lappeenranta, Finland

kalle.lipiainen@lut.fi

Abstract:

This paper investigates the fatigue strength characteristics of CO_2 laser, fiber laser and plasma cut edges of S690 and S1100 steel grades. The effect on fatigue performance of surface quality, which was examined by contact measurements and 3D scanning, residual stresses and microhardness profile, is studied and edge surface characteristics are compared for different cutting methods and 8 mm and 12 mm plate thicknesses. Four main experimental fatigue test series were performed and analyzed to estimate fatigue performance (defined as FAT classes) of the cut surface. Additional tests were conducted to study critical defects and residual stresses influence on fatigue properties. Scanning electron microscopy (SEM) revealed multiple critical locations in the specimens. Fatigue properties were characterized based on critical defects and crack initiation and propagation origins. Geometrical discontinuity points in the cut edges were found to have a significant influence on fatigue performance. It is concluded that classification of thermally cut edges by cut edge characteristics could be used in fatigue strength assessment as an alternative to standard FAT classes.

Keywords: cut edge, thermal cutting, ultra-high-strength steel, surface quality, fatigue strength

1. Introduction

Plasma, CO_2 laser and fiber laser reactive fusion cutting can be used to cut steel plate materials, although these forms of cutting have the drawback that an oxide layer has to be removed after cutting. In this study, 10 kW fiber laser cutting system was used to cut fatigue tests specimens. Used high power fiber laser enables sheets up to 12 mm thick to be cut as fusion cutting using nitrogen as an assistant gas, which improves productivity, or plates up to 25 mm thick to be cut as reactive fusion cutting using oxygen. Usage of high and ultra-high-strength steels (HSS/UHSS) has grown in recent years increasing static performance. Fatigue strength of lightweight structures is important for CO_2 emissions mitigation, and accurate assessment of fatigue strength has grown in importance. Cut edges have become an important design criteria in weight critical applications where welded joints are high frequency mechanical impact (HFMI) treated or located in low stress areas. Currently IIW recommendations [1] and Eurocode3 [2] allow nominal fatigue class FAT 125 MPa m = 3 for cut edges with corners removed, whereas FAT 180 MPa m = 5 is recommended by IIW [3] for HFMI-treated UHSS welds.

Fatigue of thermally cut edges has been studied previously using statistical evaluation of fatigue test results and high variation in fatigue capacity is observed. Runout stress range at $2{\cdot}10^6$ – 10^7 cycles between 230 MPa [4] and 520 MPa [5] has been

found with 6–15 mm thick plate specimens of laser cut HSS/UHSS. Fatigue performance has been investigated in several studies [4–8] by defining FAT values and comparing results to standards and FAT 125 MPa has been found to be conservative. In the crane industry, EN 13001 [9] is used for design, and fatigue classes are defined by considering base material (BM) yield strength and cut edge surface quality. IIW and Eurocode3 standards recommend FAT 140 MPa with m = 3, without considering material strength for ground edges, whereas crane standard EN 13001 uses SN-curve slope m = 5 and allows application of FAT classes from 140 MPa to 180 MPa depending on the yield strength for normal and according to EN9013 [10] Range 3, cut edge qualities.

Previous studies assessing fatigue in thermally cut edges have considered material yield strength and surface quality as the main influencing factors but the influence of crack propagation origin in the edge has not been reported in detail in all previous studies. Plasma cut holes were fatigue tested in [11] and crack initiation from surface defects was found with SEM. The effect on surface quality and cutting efficiency of the wavelength difference between CO_2 lasers (10.6 μm) and fiber lasers (1.07 μm) is discussed in [12]. The surface quality of fiber laser cut edges cut with fusion cutting has been found to be sufficient for butt welds without any surface treatment after cutting to increase productivity but the effect of the laser source and assistant gas on the fatigue performance of free cut edges are limited [13]. Fatigue tests in this study with high power fiber laser fusion cut UHSS edges supplement previous studies reactive fusion cut edges fatigue test results. Characterization of thermally cut edges similarly to defects in welded joints in EN 5817 [14] and by assessing the fatigue strength based on imperfections and a non-conservative FAT would increase the accuracy of fatigue life assessment [15].

In this study, crack initiation locations are characterized and other influencing factors like residual stress, burr attachment, rolled surface quality and changes in material hardness are studied for various crack initiation locations. A schematic drawing of thermal cutting is presented in Figure 1 to illustrate the terminology used in this paper.

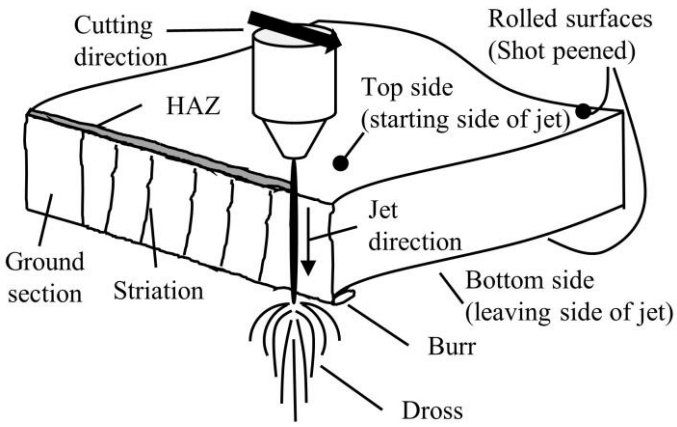

Figure 1. Schematic drawing of thermal cutting. (1 Column)

2. Specimens and test methods

Test specimens were cut from 8 mm S1100 grade steel manufactured by SSAB, and 12 mm S690QL steel plates in the rolling direction. The specimens illustrated in Figure 2 were cut were cut with fiber laser, CO_2 laser and plasma processes. In fatigue testing, the focus was on fiber laser fusion cut edges. Plasma, fiber and CO_2 laser reactive fusion cut edges were used as a comparison. Commercial cutting systems were used with manufacturers' recommended cutting parameters (Table 1). The specimens were tested in as-cut condition due to possible improvement in cutting productivity. In addition to as-cut specimens tests, S690 and S1100 fiber laser and S690 plasma cut specimens were tested to define fatigue performance improvement with burr grinding. For metallurgical analysis, the specimens were etched with 4 % nitric acid and ethanol solution. Focal point position was measured from the top of the plate and the positive direction was towards the cutting head.

Table 1. Laser cutting parameters.

Specimen	Thickness [mm]	Cutting speed [mm/min]	Power [kW]	Assistant gas	Pressure [bar]	Focal point position [mm]
S1100 – Fiber laser	8	6000	10	Nitrogen	6.5	-4
S1100 – Fiber laser	8	1900	3	Oxygen	0.5	2
S690 – Fiber laser	12	3150	10	Nitrogen	8.5	-6
S690 – CO_2 laser	12	1700	5	Oxygen	0.6	0

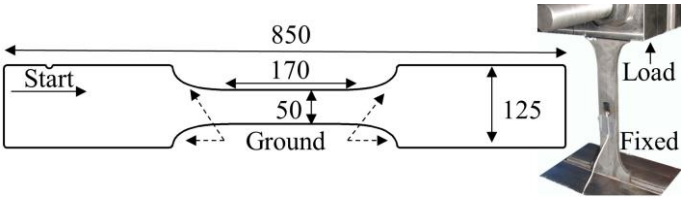

Figure 2. Geometry of cut specimen and rig attachment. (1 Column)

The S1100 surface was in as-rolled condition and the S690 was shot peened before cutting. Both steel grades were quenched and tempered. Fatigue test results and residual stress measurements for direct-quenched S960 cut edges from [16] were used to compare waterjet cutting to thermal cutting for a similar specimen and test arrangement. Static tensile tests were carried out for CO_2 laser cut S690QL and fiber laser reactive fusion cut S1100 specimens. The results of the tensile tests are presented in Table 2.

Table 2. Yield and tensile strength of materials.

Specimen	Yield strength [MPa]	Tensile strength [MPa]
S690QL	757	818
S1100	1112	1143

Surface quality of the specimens was measured by contact measurement and with a non-contact optical 3D profilometer (Keyence VR-3200). Contact measurement included six measurements from the top and bottom of the cut edge. Two specimens were measured with contact measurement for each test series. Specimens were classified to surface quality and cut edge perpendicularity Ranges according to EN 9013. Edge perpendicularity is influenced by cutting method and parameters, but it is not related to free cut edge fatigue strength. Cut surface roughness values based on contact measurements and quality classifications are given in Table 3. The visual surface quality of the test specimens is shown in Figure 3.

Table 3. Cut edge quality based on contact measurement.

Material	S690			S1100	
Cutting method	CO_2 laser O_2	Fiber laser N_2	Plasma Air	Fiber laser N_2	Fiber laser O_2
R_a Average [µm]	7	9	3	7	4
R_z Average [µm]	38	51	16	37	21
R_a Maximum [µm]	10	14	6	10	7
R_z Maximum [µm]	56	74	25	58	29
Surface quality [Range]	3	3	1	3	2
Perpendicularity [Range]	2	1	3	2	1

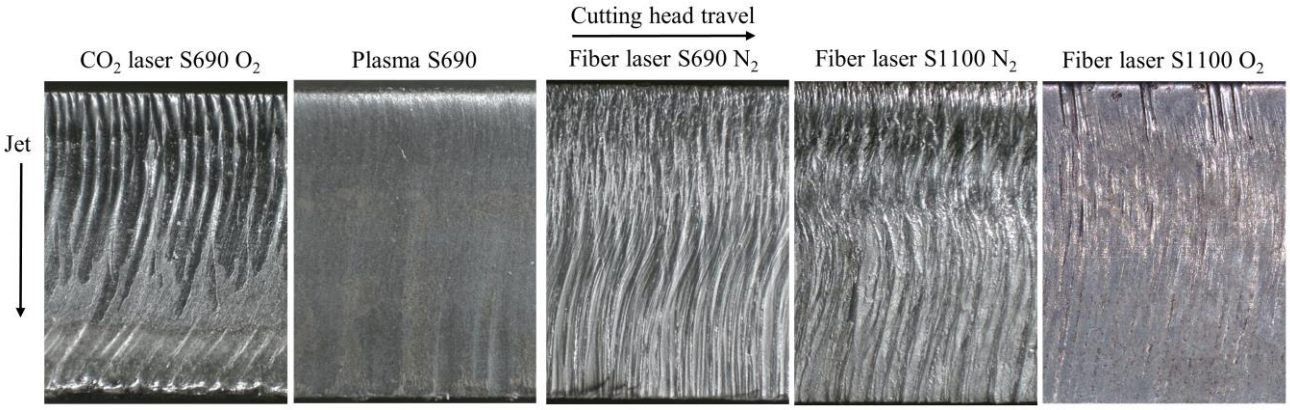

Figure 3. Surface quality of cut edges. (2 Columns)

Typical surface roughness profiles of the specimens cut and rolled edges are presented in Figure 4. The arithmetical mean height from measurement of a 5 mm length was used as a zero height. The standard R_z value does not include width data of the surface pattern, but profilometer measurements include a full two-dimensional profile of the measurement line located in critical areas. The depth and width of the defects and the interaction of the defects affect the notch stress and stress gradient. Rolled surface quality was also measured and was found to be an important factor for fatigue performance as discussed in Chapter 4.

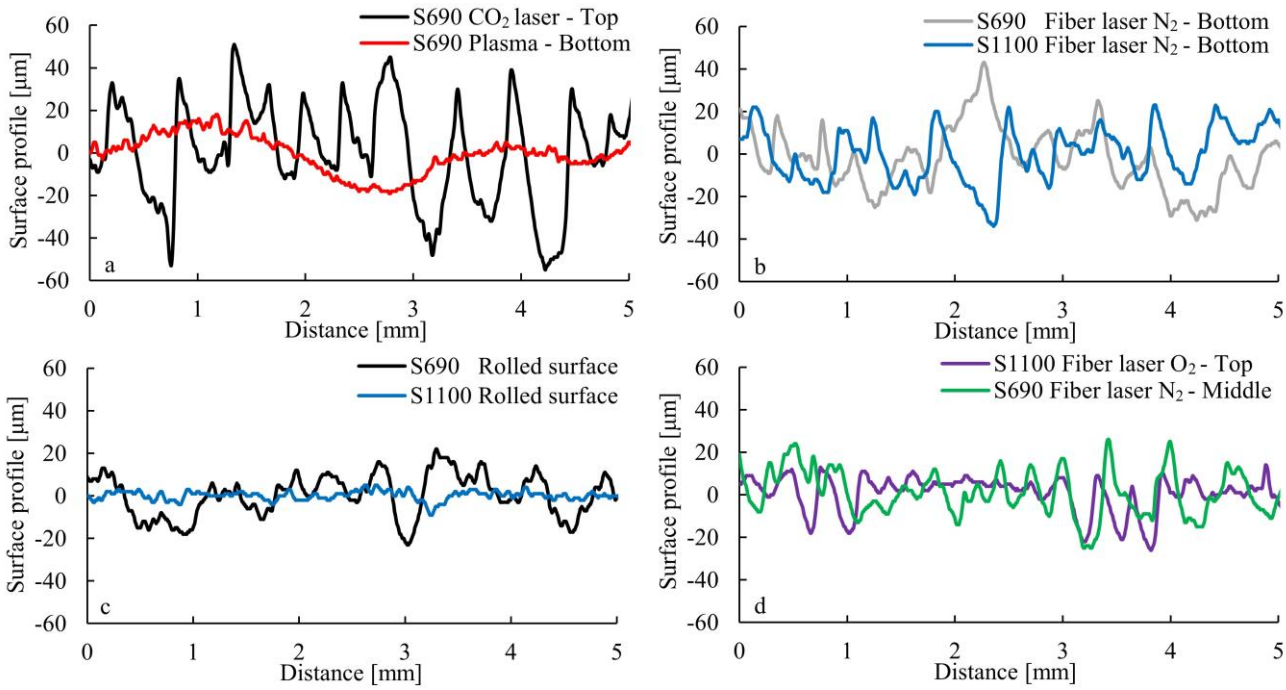

Figure 4. Surface roughness profile of (a) CO_2 laser and plasma cut specimens, (b) fiber laser cut specimens, (c) rolled surfaces, and (d) Burr removed S690 and reactive fusion cut S1100 specimens. (2 Columns)

Fatigue classes for cut edges are presented in Table 4 to demonstrate differences in the standards. The EN 13001 allows the highest FAT classes in as-cut condition for cutting methods without burr attachment. After burr removal, the plasma cut edge has the highest FAT class due to Range 1 surface quality classification. EN 13001 recommends significantly higher FAT classes for machined edges compared to thermally cut edges.

Table 4. FAT classes for different cut edge conditions

Material		S690			S1100	
Standard	Condition	CO_2 laser O_2	Fiber laser N_2	Plasma Air	Fiber laser N_2	Fiber laser O_2
IIW m = 3 [MPa]	As-cut			100		
	Corners removed			125		
	Edges ground			140		
EN 13001 m = 5 [MPa]	As-cut	180	140	140	180	200
	Burr removed	180	180	225	180	200
	Machined		280		315	

Experimental fatigue tests were conducted with uniaxial constant amplitude loading. Stress ratios of R = 0.1 and R = 0.4 were used for S690 and R = 0.1 and R = 0.5 for S1100 specimens. Two different stress ratios were used to evaluate the effect of loading condition to fatigue performance. Tests were stopped when specimen's maximum displacement exceeded 3 mm or runout limit of $2 \cdot 10^6$ cycles was achieved. Fatigue testing of the edge of the CO_2 laser cut S690 specimen was not possible with R = 0.5, due to runout, when stress was limited to 95 % of the nominal yield strength of material. Typical out-of-plane deflection of the specimens after cutting was 1 mm with 0.5 mm variation. Bending stress due to the curvature of the specimen and attachment to the test rig was measured with a strain gauge from the center of the specimen at the bottom side and varied between 2–20 MPa.

3. Test results

3.1 Metallurgy

According to the EN 1090 [17], the hardness of free thermal cut edges can be measured with the HV10 hardness test at a ground cut edge where some indentations of the cut surface are still visible. For carbon steels with yield strength of 460 MPa or higher, the maximum allowed hardness is 450HV. The hardness of the cut edges was measured from the cross section with five indentations inside the heat affected zone (HAZ) per specimen. Due to narrow HAZ, the HV5 method was used for the S690 specimens and HV3 for the S1100 specimens. Based on the hardness measurement results presented in Table 5, both the S690 and the S1100 specimens exceeded the maximum permitted hardness given in EN 1090. The plasma cut edge had a smooth surface and a hardness test was also conducted on the cut edge directly. Without grinding, 600 HV hardness was measured corresponding to microhardness measurement at 35 µm distance from the cut edge. After fine grinding, hardness was measured with standard EN 1090 method and the results were similar to HV5 measurements inside the HAZ and microhardness measurements at 75 µm distance from the cut edge.

Table 5. Vickers hardness inside HAZ and base material hardness.

Material and test method	S690 - HV5				S1100 - HV3		
Cutting method	CO_2 laser O_2	Fiber laser N_2	Plasma Air	BM	Fiber laser N_2	Fiber laser O_2	BM
Max. hardness [HV]	456	462	485	291	500	479	391
Avg. hardness [HV]	443	451	463	284	484	472	379

Microhardness was measured from the centerline of the specimen. The first point was measured with HV0.05 method at distance of 35 µm distance from the cut edge whereas following points (75–500 µm) were measured with HV0.2 method. The CO_2 laser cut specimen was also measured from the top side of the specimen close to the most significant striations. Measured microhardness profile presented in Figure 5. Significantly increased hardness values were measured close to the cut edge of the laser and plasma cut specimens. The width of the HAZ varied from 0.20 mm to 0.35 mm at the specimen centerline and the width of the HAZ correlated with the cutting speed. The cutting speed of fusion cut S1100 was fastest and this specimen had the narrowest HAZ.

The HAZ was narrow at the top of the laser cut edges and hardness increase outside HAZ at the top of the specimen can be explained by increased temperature near the cutting kerf and shot peening the rolled surface but also small decrease in hardness was measured at 0.25 mm distance from cut edge close to crack initiation in fatigue testing. Microhardness measurement of base material gives a good estimation of base material hardness at 0.35–0.5 mm distance from the cut edge. Hardness corresponding 1000–1400 HV was found for a 5–10 µm thick recast layer at the cut edge and 600–800 HV up to 50 µm distance from S355, S690 and S890 laser and plasma cut edges with a nanoindentation test [18]. Peippo et al. [19] reported 460-680 HV hardness with HV0.2 method at 0.05-0.1 mm distance from plasma and laser cut edges with S235, S355 and S960 materials.

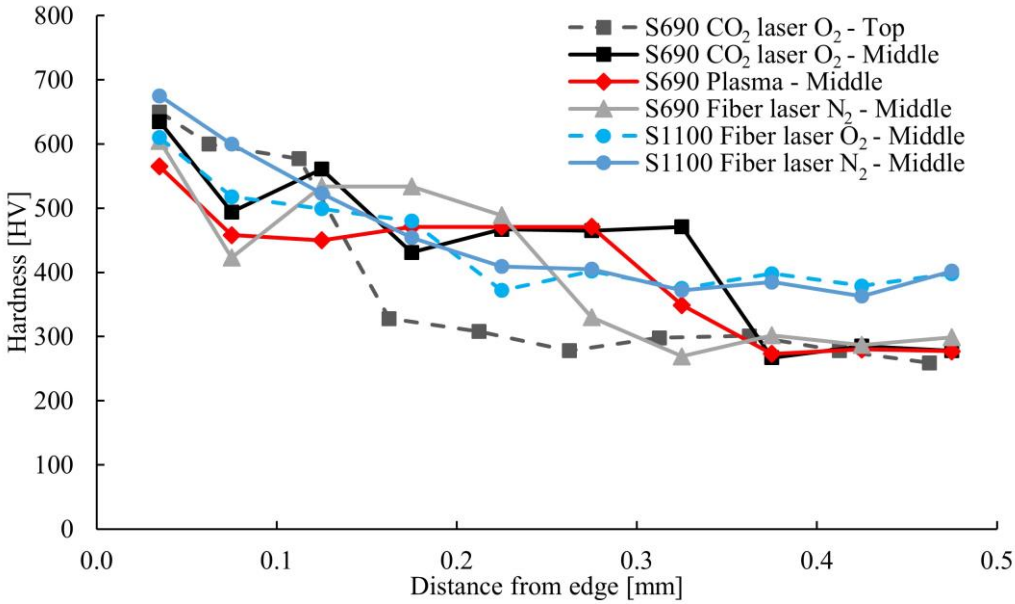

Figure 5. Microhardness distributions of cut edges. (1.5 Columns)

Scanning electron microscopy (SEM) with secondary electron (SE) and backscattered electron (BSE) detection was used to evaluate the microstructure and metallurgical properties of the laser cut edges. Cross sections of the CO_2 laser and fiber laser cut edges are presented in Figure 6. The recast layer is clearly visible in the CO_2 laser cut edge (Figure 6a), whereas a recast layer where no grain boundaries are visible was not detected in fusion cut edges. A molten layer of 30 µm width is visible in Figure 6b. A molten layer of 50 µm width was found in the S690 specimen. Transition from HAZ to BM was sharp and no significantly softened zone was detected in the microhardness measurements or cross section in SEM inspection.

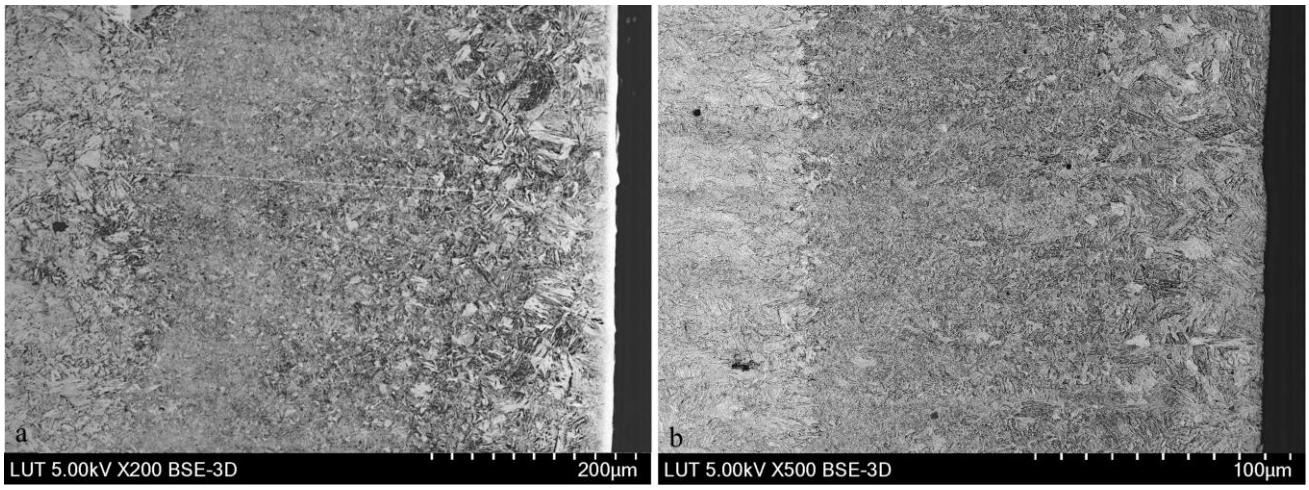

Figure 6. Cross section of (a) S690 CO_2 laser cut edge and (b) S1100 fiber laser cut edge. (2 Columns)

Chemical composition, excluding carbon from analysis, with energy dispersive X-ray spectroscopy (EDS) from single point measurements is presented in Table 6. Point analysis indicated significant change in CO_2 laser cut edge whereas only minor changes in fusion cut specimens. EDS mapping was performed for the CO_2 laser cut edge and the results are presented in Figure 7 showing a SE image of the area. The recast layer was found to have changed elemental composition, but chemical composition was changed compared to the BM even at a distance of 50 µm from the cut edge. The oxide layer was removed in etching and the recast layer without grain boundaries is visible in the SE image.

Table 6. Elemental analysis with EDS. Results in mass-% at the edge and 0.1 mm distance from the edge.

Specimen	Location	Element [m-%]					
		Al	Si	Cr	Mn	Fe	Mo
CO_2 laser S690	Edge	0.2	0.1	0	0.3	99.3	0.2
	0.1 mm from edge	0.4	0.5	0.2	1.2	97.6	0.1
Fiber laser S690	Edge	0.3	0.4	0.2	1.1	98.0	-
	0.1 mm from edge	0.3	0.5	0.3	1.0	97.9	-
Fiber laser S1100	Edge	0.3	0.3	1.3	1.3	95.6	0.4
	0.1 mm from edge	0.3	0.2	1.4	1.3	95.6	0.4

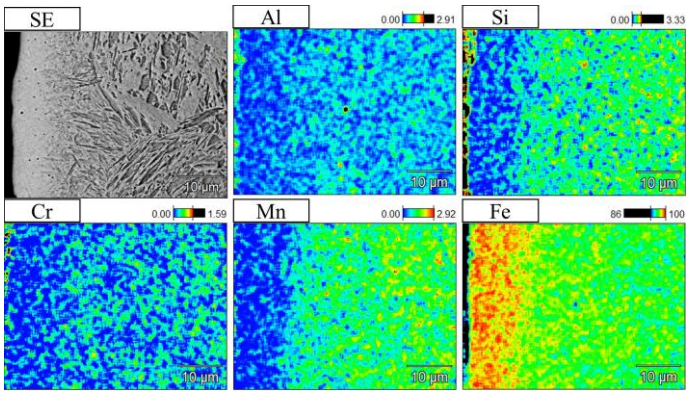

Figure 7. SE-image and EDS-analysis of CO_2 laser cut edge. (1 Column)

Residual stresses and Full Width at Half Maximum (FWHM) values were measured with a Stresstech Xstress G3 diffractometer using X-ray diffraction (XRD). FWHM values are measured from the XRD intensity profile width and values represent hardness, microstresses and plastic deformation. FWHM values can be used to complement microhardness measurements in cut edge characterization although exact correlation between FWHM and hardness values is not known. Leitner et al. [20] reported FWHM values for welded joints of steel grades of S355 and S960 where HV3 hardness at the weld toe area varied from 165 HV to 360 HV [21]. FWHM values of 3.5° (S355) and 4.25° (S960) were obtained for HFMI-treated weld toes, whereas FWHM values for as-welded joints were close to base material values of 1.75° and 2.5°. FWHM of cut edges were studied in [22].

Residual stresses at the middle of the cut edge, parallel to loading, and FWHM values are presented in Table 7. Specimens were in the as-cut condition except the 10 % citric acid treated S1100 specimens. Acid treatment has been found to have only a minor effect on the residual stress state of UHSS [23] but the acid-treated specimens were the only series in which compressive residual stresses were consistently measured at the cut edge. Acid treatment was used to prevent fretting fatigue to occur in gripping areas of the specimens when long cycle regime fatigue tests were performed. Tensile residual stresses measured at the cut edges were higher in the S690 than S1100 specimens.

Table 7. Residual stresses and FWHM values at the middle of the cut edges.

Material	S690			S1100	
Cutting method	CO_2 laser O_2	Fiber laser N_2	Plasma	Fiber laser N_2	
				As-cut	Acid treated
Avg. residual stress [MPa]	210	119	146	76	-6
Min. residual stress [MPa]	117	-28	76	28	-32
Max. residual stress [MPa]	451	252	342	181	17
Avg. FWHM [°]	5.06	3.66	5.02	4.22	4.35

Residual stresses and FWHM values were also measured for milled S690, waterjet and CO_2 laser cut S960, and fiber laser fusion cut S1100 specimens. Average residual stresses parallel to the rolling and loading direction and FWHM values at the middle of the cut surface are presented in Table 8. Compressive residual stresses were found from the middle of rolled surfaces

in S690, S960 and S1100 specimens and shot peening was found beneficial for rolled surface residual stress state. FWHM values of 2.4° (S960) and 2.2° (S1100) were found from rolled surfaces. Heat input decreased FWHM values in the shot peened S690 specimens. An average FWHM value of 2.1° was measured at the heat affected area in the plasma cut and milled specimen whereas FWHM value of 3.1° was measured from the middle of the shot peened surfaces of specimens.

Table 8. Average residual stresses and FWHM values of additional specimens.

Material	S690	S960		S1100
Cutting method	Milled	CO_2 laser O_2	Waterjet	Fiber laser O_2
Avg. residual stress [MPa]	214	190	-319	-4
Avg. FWHM [°]	3.00	5.27	3.77	4.87

The residual stress profile of the CO_2 laser and plasma cut S690 specimens was measured using XRD and electropolishing. For comparison, the residual stress profile of a CO_2 laser cut specimen was measured with a Stresstech Prism system utilizing the electronic speckle pattern interferometry (ESPI) hole drilling method. Measurements were made at the middle of the cut edges in both the parallel (0°) and transverse (90°) to loading directions. The residual stress profile is shown in Figure 8a and FWHM profile from XRD measurements in Figure 8b.

High tensile residual stresses were measured from BM, with maximal values being located at 0.5 mm distance from the cut edge. With XRD technology, the measurement depth was limited to 0.5 mm but ESPI measurements complemented the measurements. The ESPI results showed that after a high peak of tensile residual stresses, residual stresses decreased steadily to close to zero at 2 mm distance from the edge. Similar behavior of a high tensile residual stress peak in base material has been found in several studies [5,18,24].

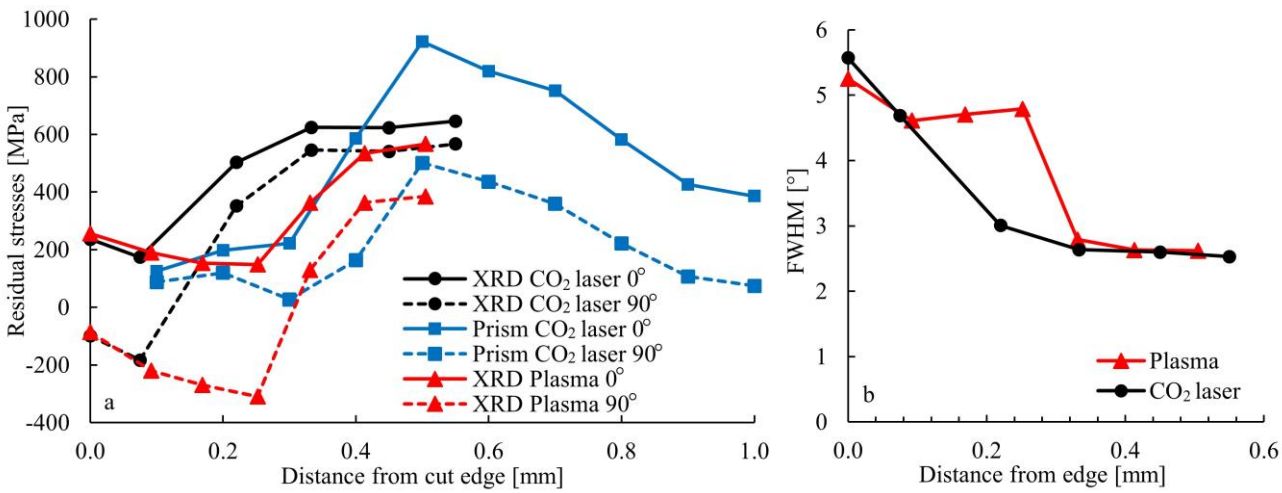

Figure 8. Residual stress profile of (a) CO_2 laser and plasma cut S690 specimens and (b) FWHM values from XRD measurements. (2 Columns)

3.2 Fatigue tests

Fatigue test results were analyzed using Deming regression, i.e. the minimum sum of perpendicular distances method (MSSPD). A nominal stress approach was used, and all FAT classes were calculated with 50 % failure probability. Fatigue

test results are shown in Figure 9 and ground section failures or runouts are marked with arrows and excluded from SN-curve fitting. Results are separated for R = 0.1 (filled markers) and R = 0.4–0.5 (unfilled markers) stress ratios and additional tests are identified with crosses and pluses. S690 CO_2 laser cut edges had the best fatigue performance. Fiber laser fusion cut S1100 had similar fatigue performance to plasma cut S690 edges.

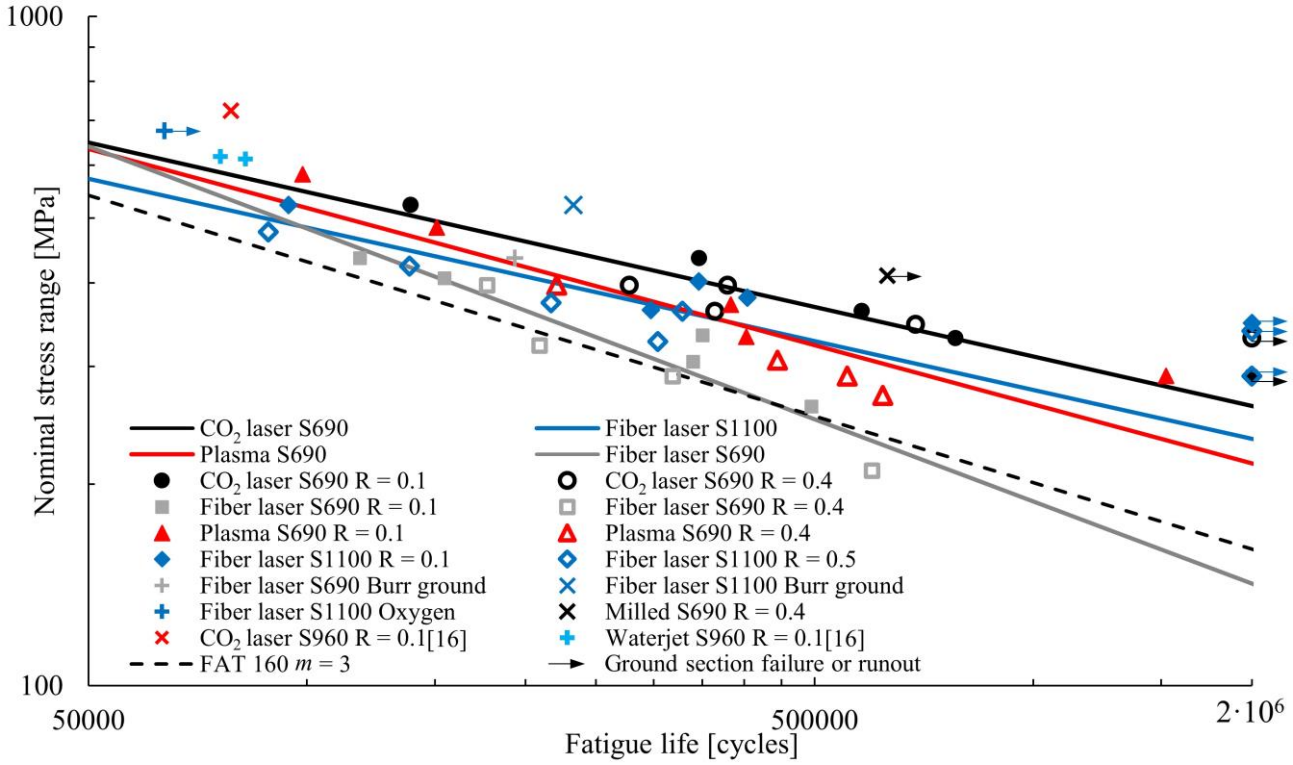

Figure 9. Fatigue test results with R = 0.1 and R = 0.4–0.5 stress ratios. (2 Columns)

FAT classes were calculated using fixed slopes of m = 3 and m = 5 to compare results to standard FAT classes. The calculated FAT classes and the slopes of the SN-curves are presented in Table 9. The CO_2 laser cut S690 edge has the highest FAT class with all three curve fitting procedures. Highest runout stress range was 350 MPa for the fiber laser cut S1100 specimen and 330 MPa for the CO_2 laser cut S690 edge, respectively. Plasma cut edge failure was experienced at $1.5 \cdot 10^6$ cycles with 290 MPa stress range. Similar to other studies, the test results showed better fatigue strength after 10^6 cycles than estimated with SN curves [5–8].

Table 9. Calculated mean and characteristic FAT classes with free and fixed slopes.

Cutting method	Assistant gas	Material	Stress ratio [-]	MSSPD Slope [-]	FAT [MPa]					
					50% MSSPD	97.7% MSSPD	50% m = 5	97.7% m = 5	50% m = 3	97.7% m = 3
CO_2 laser	O_2	S690	0.1 & 0.4	4.07	262	232	282	247	227	192
Fiber laser	N_2	S690	0.1 & 0.4	2.45	142	120	215	160	165	137
Plasma	Air	S690	0.1 & 0.4	3.41	215	170	252	191	201	157
Fiber laser	N_2	S1100	0.1 & 0.5	4.12	234	198	259	216	188	148

Additional fatigue tests were conducted with high stress range and the results are presented in Table 10. The plasma cut specimen with a milled surface had high fatigue performance and failure occurred in the specimen's ground section and not at the milled surface. Fatigue performance of the fusion cut S690 specimen improved with burr grinding. The crack propagated from a cut edge defect, but the fatigue performance was still lower than the plasma cut edge specimen with a burr attached. Reactive fusion cutting process was beneficial for fatigue performance of fiber laser cut S1100 edges although failure occurred from specimens ground section. The surface quality of the burr-removed fusion cut S690 specimens and reactive cut S1100 specimens in critical locations was similar (Figure 4d) but reactive fusion cut edge had significantly higher fatigue performance.

The S960 specimens had high fatigue performance but low surface quality in terms of R_z values, and classification of surface quality was Range 3 (CO_2 laser) and Range 4 (waterjet) according to EN 9013. The fusion cut and burr ground S1100 specimen had high fatigue performance, although the fatigue crack initiated at the cut edge from a defect similarly to the burr ground S690 specimen. Fatigue performance was highly dependent on the assistant gas used in laser cutting although the surface roughness profile influenced fatigue performance.

Table 10. FAT classes of additional fatigue tests with fixed slopes. S960 data from [15].

Cutting method	Assistant gas	Treatment	Material	Stress ratio [-]	FAT m = 5 [MPa]	FAT m = 3 [MPa]	Note
Plasma	Air	1 mm milling	S690	0.4	325	279	Ground section failure
Fiber laser	N_2	Burr removed	S690	0.1	273	200	
Waterjet	-	No	S960	0.1	323	210	Two specimens
CO_2 laser	O_2	No	S960	0.1	379	246	
Fiber laser	N_2	Burr removed	S1100	0.1	340	255	
Fiber laser	O_2	No	S1100	0.1	339	214	Ground section failure

3.3 Crack initiation

Fracture surfaces were examined with SEM to determine critical locations of fatigue crack initiation at the cut edge. Discontinuity points and defects were found in fiber laser and plasma cut specimens, whereas CO_2 laser cutting with oxygen did not result in any sharp defects in the cut edge. Critical defects of each cutting method are illustrated in the schematic drawing in Figure 10. Variation between different failure modes was not found inside fatigue test series. However, multiple crack initiation location along specimen's length were observed in fusion cut specimens. Detailed fracture surfaces are presented in Figures 11–14, where jetting direction is from top to bottom and crack initiation locations are circled.

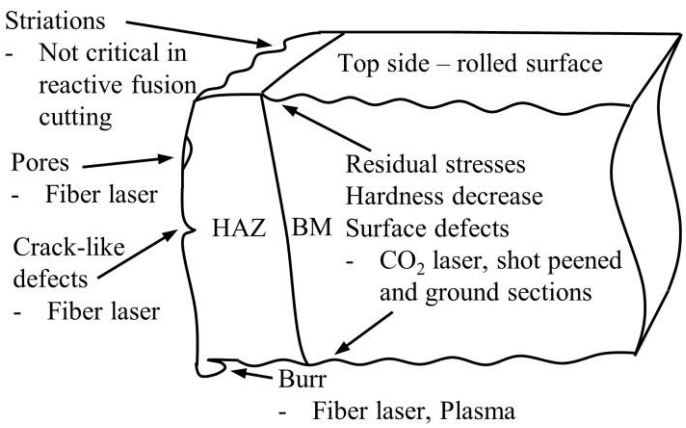

Figure 10. Schematic drawing of critical locations of fatigue crack initiation. (1 Column)

Fractures propagated from the burr of the fiber laser cut edge, as can be seen in Figure 11. The effect of plate thickness on burr formation was significant, but sharp discontinuity points were non-dependent on burr size in fusion cut edges cut edges. Fracture surfaces indicated crack propagation from the burr area in plasma cut specimen, but the burr was found not found to form as sharp or detrimental discontinuity points as in fiber laser fusion cut edges.

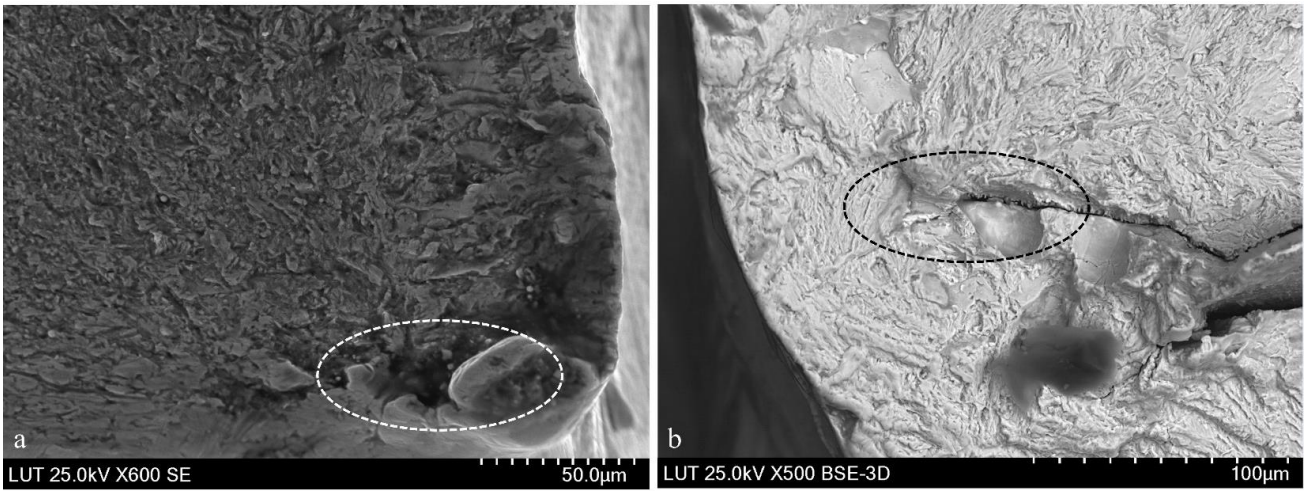

Figure 11. Fracture surfaces and burrs of (a) fiber laser cut edges S690 and (b) S1100 (2 Columns)

The crack initiated in the base material in the CO_2 laser cut edge. The location and mechanism for crack initiation varied according to loading. At high stress range, the crack initiated at the rolled surface on the top side, whereas below 370 MPa stress range the crack initiated at the rolled surface on the bottom side. These two failure modes are shown in Figure 12. Shot peening of the plate material before cutting was detrimental because it induced stress concentration and compressive residual stresses were relaxed due to heat input. Sperle [8] found that the balance between the cut edge and rolled surface quality affected fracture initiation, together with bending stress induced from out-of-plane deflection of the specimen. Fracture surfaces and the test results of this study support the argument that they are influencing factors for crack initiation and growth, together with surface geometry, including rolled surfaces, microhardness and residual stress profile.

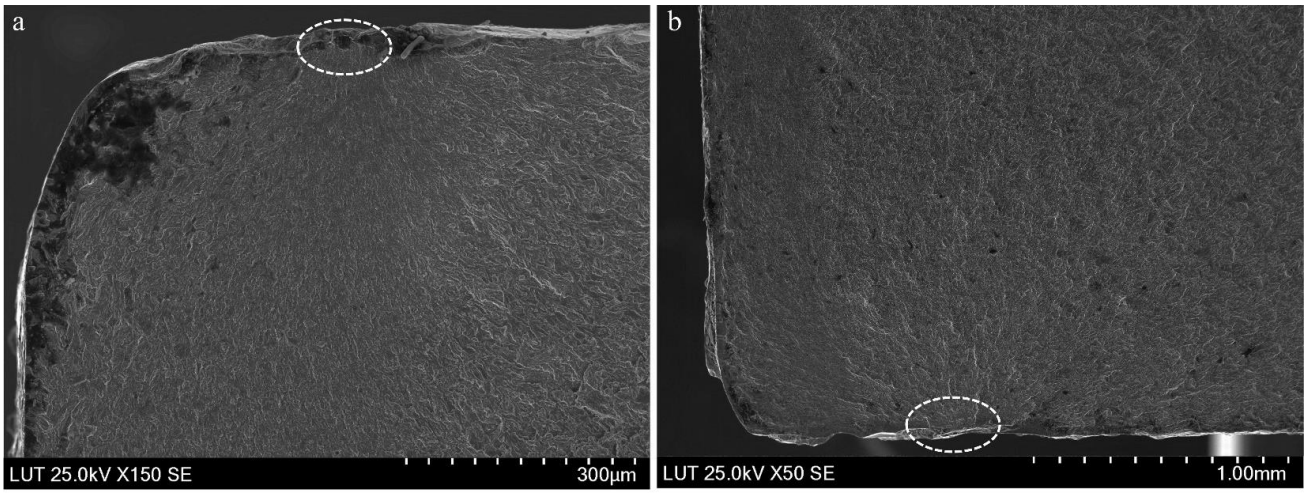

Figure 12. Crack initiation locations of CO_2 laser cut edges (a) top of the plate and (b) bottom of the plate. (2 Columns)

Fiber laser fusion cut S690 and S1100 edges and plasma cut S690 edges were studied also in burr-ground condition. Fatigue life from the test result closest to 10^5 cycles fatigue life was used as a comparison value and burr-ground specimens were tested with corresponding loading. The effect of burr grinding on fatigue life is shown in Table 11. Burr removal had a more significant effect on the fusion cut UHSS specimen than the HSS specimen. Failure of the plasma cut and burr-ground specimen occurred in the ground section and crack initiated from notches in the shot peened surface on the top side of the specimen outside the HAZ.

Table 11. Effect of burr grinding on fatigue life.

Specimen	Fatigue life improvement
S690 Plasma	6.3 %
S690 Fiber laser N_2	63 %
S1100 Fiber laser N_2	147 %

On inspection, defects from fusion cutting were found in the cross section of the S690 cut edge. Crack-like defects act as an initial defect for fatigue crack growth. The cross section including crack-like defect and fracture surface of the fiber laser fusion cut S690 specimen are presented in Figure 13. The critical defects in the S690 specimen were located in the middle of the cut surface, whereas in the S1100 specimen the defects were found at 2 mm distance to the top of the specimen. The defects were located in a region of turbulent assistant gas flow.

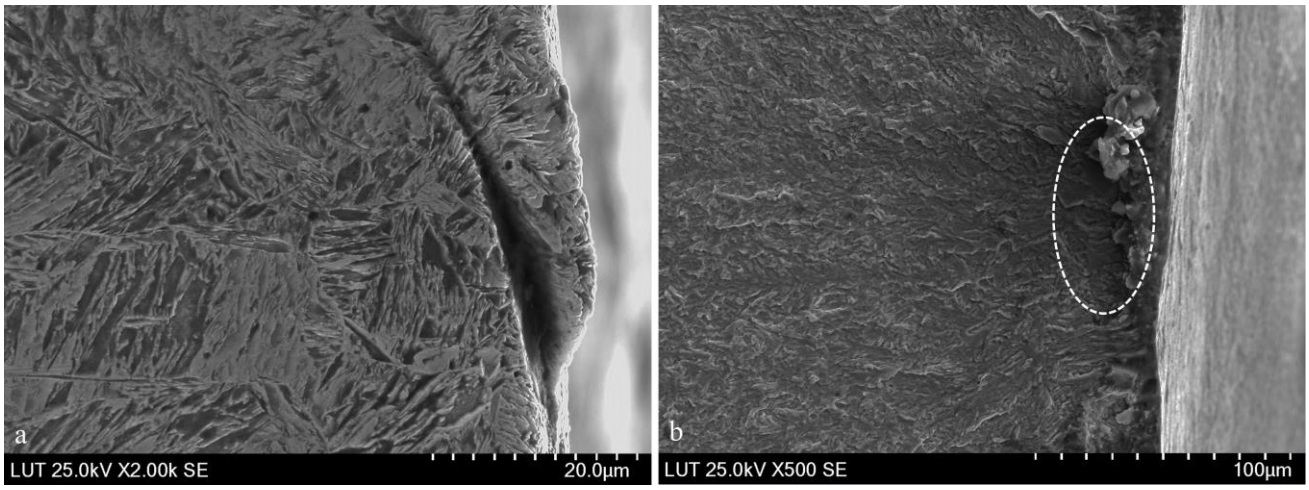

Figure 13. (a) Defect in the fiber laser fusion cut S690 specimen and (b) detail from the crack origin fracture surface (2 Columns)

The defects in the cut edge were different in the S1100 specimen. A molten and solidified layer and porosity are clearly visible in Figure 14. The crack initiation area is located at a discontinuity point at 30 µm distance from the cut edge. Pore-like defects were not found to be as detrimental as crack-like defects in the thicker S690 specimen. Table 12 presents EDS measurements near crack initiation area. Oxygen and an increased amount of silicon and manganese were found in the narrow boundary layer between the molten layer and cut edge, whereas the chemical composition on both sides of the boundary layer was close to that of the BM.

Table 12. EDS measurements from S1100 fracture surface.

Point	Element [m-%]							
	O	Al	Si	Cr	Mn	Fe	Ni	Mo
1	-	0.4	0.3	1.5	1.3	95.2	0.9	0.5
2	6.1	0.9	2.1	1.5	3.6	84.7	0.6	0.4
3	-	0.5	0.3	1.5	1.4	95.0	1.0	0.5

Figure 14. Fracture surface and EDS measurement points of a burr ground S1100 specimen. (1 Column)

4. Discussion

Lack of published studies exists in terms of the fatigue performance of fusion cut structural steels but low-to-mid power fiber laser fusion cutting fatigue studies are reported for stainless steels. Pessoa et al. [25] found cut edge criticality for burr- and pore-like defects in AISI304 fiber laser fusion cut edges, where pores were located within 50 µm distance from cut edge. With a polished cut edge, fatigue crack grew from non-metallic inclusions. Fatigue performance increased only slightly after burr removal but significantly after polishing the cut edge.

Fatigue strength of high-strength duplex grades 2205 and 2507 with ground (laser and waterjet cut), laser cut, waterjet cut and plasma cut edges were tested in [26,27] and the fatigue test results with $R = 0.1$ compared to FAT 280 MPa $m = 5$ are presented in Figure 15. Runout stress range of 360–410 MPa at $5 \cdot 10^6$ cycles was found. Fatigue test results suggests that the fatigue performances of duplex and structural steel cut edges are comparable.

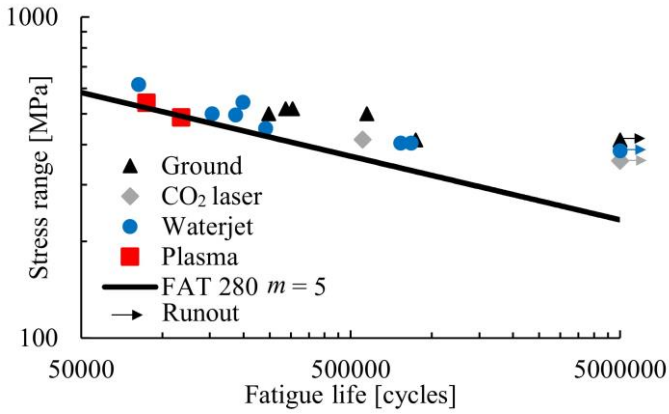

Figure 15. Duplex cut edge fatigue test results. Data from [26,27]. (1 Column)

Fiber laser fusion cut edges tested in this study resulted significantly lower fatigue performance than in laser cut UHSS specimens in [5,7,8] due to cut edge defects. The reactive fusion cut S1100 edge had better fatigue performance than the fusion cut edge in as-cut condition, due to smaller burr and lower cut edge induced notch factor at the bottom of the cut edge. Local surface quality and defects are influenced by the cutting process. The highest notch factor in fusion cutting is located at the burr area, whereas reactive fusion cutting produces significant striations at the top of the cut edge and notch stress is small in the burr area. Burrs in fiber laser fusion cut edges reduced fatigue life significantly, but plasma cut edges had good fatigue performance with burrs attached.

The surface of the CO_2 laser cut edge had the highest surface roughness in terms of R_z value measured with optical measurements. Nevertheless, CO_2 laser cut edges provided good fatigue performance in as-cut condition. Burr-removed fusion and as-cut reactive fusion cut S1100 specimens had the best fatigue performance. The good fatigue performance of reactive fusion cut edges can be explained by the hardness of the cut edge correlating with fatigue strength, as explained in [28]. The accuracy of hardness measurement decreases with low indentation weight, but it is necessary to use near the cut edge surface

and the measured microhardness distributions seemed reasonable and consistent. The microhardness profile corresponded in the HAZ and BM HV3, and HV5 hardness measurements and microhardness profile had a similar trend to the FWHM profile in plasma and CO_2 laser cut S690 specimens. Nanohardness measurements closer to the cut edge would have been beneficial for cutting method comparison. Residual stress distribution was measured from the centerline of the specimen but distribution in the thickness direction is not known. Fatigue tests indicated that tensile residual stresses and relaxation has an influence on fatigue performance in the high cycle regime.

Increased hardness in the cut edge seems beneficial for fatigue performance. Diekhoff et al. [6] conducted microhardness tests for oxy-fuel cut S960 edges and found out that hardness close to the cut edge was lower than base material hardness. Low surface hardness suggests that the initiation mechanism for fatigue failure of oxy-fuel cut edges is different from plasma, and laser cut edges. Waterjet cut S960 edges had good fatigue performance because low surface quality was compensated by compressive residual stresses, which were also found in [7], instead of increased hardness due to heat input and relatively fast cooling at the cut edge. FHWM values suggested that there was increase in hardness also in waterjet cut edges. Uniform cut edges had better fatigue performance than the tapered ground section in several fatigue tests. The crack initiation point of ground section failures was located at rolled and shot peened surfaces in the S690 specimens. The fatigue test results indicate that base material hardness and surface quality determine the ultimate fatigue capacity of laser and plasma cut edges if the cut edge is uniform.

The results from this study suggest that standardized cut edge classification by cut edge characteristics should be considered instead of merely surface quality measured by R_z value. The most important factors for thermally cut edge characterization indicated by this study are hardness at the cut edge induced by the cutting method and microscopic defects and burrs in fusion cut edges. The balance between the cut edge and rolled surface quality is important for optimal fatigue performance, and residual stresses induced by cutting and pre- and post-treatments should also be considered.

UHSSs provide the best fatigue performance because of the high base material hardness. The highest fatigue performance was found with reactive fusion cut S960 specimen. According to this study, the full weight saving potential of UHSSs in fatigue loaded cut structural members is not enabled with fiber laser fusion cutting. UHSSs are beneficial from the productivity perspective as fiber laser fusion cutting can be used with thinner plates. In this work, similar static and fatigue performance in as-cut condition after $5 \cdot 10^5$ cycles was achieved with almost two times higher cutting speed and without visible burr attachment when 12 mm HSS was changed to 8 mm UHSS. Plate thickness and steel grade had strong correlation to fusion cut edge fatigue performance when the burrs were ground, although similar defects were found for cut edges with different thicknesses. Fiber laser fusion cut S1100 specimens characteristic fatigue performance in as-cut condition exceeded HFMI treated welded joint nominal FAT class of 180 MPa $m = 5$ and increase in cutting efficiency could be utilized in welded UHSS structures.

Further studies are needed on fusion cut surfaces with high pressure and fully laminar assistant gas flow to compare the effect of the assistant gas on fatigue performance. The effect of residual stress on fatigue performance could be studied with similar CO_2 laser cut specimens that are shot peened after cutting to induce compressive residual stresses. Fiber laser technology is used in tube or robotic arm cutting systems and the results of coupon specimens could be generalized to perforated hollow section tubes as presented in [29].

5. Conclusions

Fatigue of thermally cut edges is a complex phenomenon and different cutting methods induce different characteristics in the cut edges. In this study, it was found that the cutting process and cut edge defects had a more significant influence on fatigue performance than the cut edge surface quality measured by R_z and R_a. It is concluded that instead of surface quality, fatigue performance could be assessed based on the characteristics of the cut edge. The results suggest that burr attachment has the most significant influence on fatigue performance. When the burr is removed from the fiber laser fusion cut edge, fatigue performance was limited by defects on the cut edge, whereas neither concerns were present with CO_2 laser reactive fusion cutting and rolled surface quality had significant effect on fatigue strength.

The fatigue performance of the as-cut specimens exceeded IIW FAT class 100 MPa m = 3 significantly. Despite major burr attachment in fiber laser fusion cut S690, the as-cut specimens exceeded FAT 125 MPa m = 3 that is recommended for cut edges corners removed. Characteristic FAT values for as-cut specimens varied from 137 MPa to 192 MPa with m = 3. EN 13001 standard FAT classes in as-cut condition were also found conservative with estimated characteristic FAT values from 160 MPa to 247 MPa with m = 5. In the long cycle regime after 10^6 cycles, the fatigue performance estimated by FAT class causes unused potential because the runout limits suggest significantly higher fatigue performance than the calculated SN-curves.

The influence of surface quality on fatigue performance is compensated in reactive fusion cut edges by a thin increased hardness layer and a uniform cut edge. Burrs defined fatigue performance when present but with microscopic burrs, fatigue performance remained at a high level. Characterization of the cutting method can enable the most appropriate method for an application to be selected. Fatigue assessment considering local material properties, residual stress state and true surface quality and product geometry could be developed for thermally cut edges.

Acknowledgements

The authors wish to thank Business Finland for funding through the ISA project and SSAB Europe for providing materials for experimental tests.

References

1. Hobbacher A. 2016. Recommendations for Fatigue Design of Welded Joints and Components.
2. SFS-EN 1993-1-9, Eurocode 3: Design of steel structures. Part 1-9: Fatigue, Helsinki: SFS Finnish Standards Association.
3. Marquis G & Barsoum Z. 2016. IIW Recommendations for the HFMI Treatment.
4. Cicero S, García T, Álvarez J.A, Martín-Meizoso A, Bannister A & Klimpel A. Definition of BS7608 fatigue classes for structural steels with thermally cut edges
5. Laitinen R, Valkonen I & Kömi J. 2013. Influence of the base Material Strength and Edge Preparation on the Fatigue Strength of the Structures Made by High and Ultra-high Strength Steels. Procedia Engineering 66. pp. 9.
6. Diekhoff P, Hensel J, Nitschke-Pagel T & Dilger K. 2019. Fatigue strength of thermal cut edges—influence of ISO 9013 quality groups. Welding in the World. pp. 14.
7. Stenberg T, Lindgren E, Barsoum Z & Barmicho I. 2017. Fatigue assessment of cut edges in high strength steel - Influence of surface quality. Materials Science & Engineering Technology Volume 48, Issue 6 pp. 21.
8. Sperle J.O. Influence of Parent Metal Strength on the Fatigue Strength of Parent Material with Machined and Thermally Cut Edges. Welding in the World, vol. 52, no. 7, pp. 79-92, 2008.
9. EN 13001-3-1-2018, Cranes, General design, Part 3-1: Limit states and proof competence of steel structure., CEN European committee for standardization.
10. EN ISO 9013:2017. Thermal cutting. Classification of thermal cuts. Geometrical product specification and quality tolerances.
11. Jiménez-Peña C, Goulas C, Rossi B, Debruyne D, Influence of hole-making procedures on fatigue behaviour of high strength steel plates, Journal of Constructional Steel Research, 2019, 158, 1-14
12. Mahrle A & Beyer E. 2009. Theoretical aspects of fiber laser cutting. Journal of Physics D: Applied Physics 2009, Vol.42(17), p.175507 (9pp).
13. Sokolov M, Salminen A, Somonov V & Kaplan A. 2012. Laser welding of structural steels: Influence of the edge roughness level. Optics and Laser Technology Vol. 44, Iss. 7, (Oct 2012): 2064-2071.
14. EN ISO 5817:2014. Welding — Fusion-welded joints in steel, nickel, titanium and their alloys (beam welding excluded) — Quality levels for imperfections
15. Hobbacher A & Kassner M. 2012. On Relation Between Fatigue Properties Of Welded Joints, Quality Criteria and Groups in ISO 5817. Welding in the World 2012, Vol.56(11), pp.153-169.
16. Riski J. 2017. Low-cycle fatigue of S960 [Master’s thesis] pp.100.
17. SFS-EN 1090-2 + A1, Execution of steel structures and aluminium structures. Part 2: Technical requirements for steel structures. Helsinki: SFS.

18. High performance cut edges in structural steel plates for demanding applications, Final report, RFSR-CT-2012-00027.2016
19. Peippo J, Björk T & Nykänen T. 2018. A novel method for fatigue assessment of steel plates with thermally cut edges. Welding in the World. January 2018, Volume 62, Issue 1.
20. Leitner, M, Khurshid, M & Barsoum, Z. 2017. Stability of high frequency mechanical impact (HFMI) post-treatment induced residual stress states under cyclic loading of welded steel joints. Engineering Structures 143. p. 589–602.
21. Leitner M, Stoschka M & Eichlseder W. Fatigue enhancement of thin-walled high-strength steel joints by high frequency mechanical impact treatment.Weld World 2014;58(1):29–39.
22. Z.D. Sheng, C. Altenbach, U. Prahl, D. Zander, W. Bleck, Effect of cutting method on hydrogen embrittlement of high-Mn TWIP steel, Mater. Sci. Eng. A 744(2019) 10-20.
23. M. Dabiri, T. Skriko, T. Björk. 2015. Preparation of S960QC steel specimens for fatigue testing: Effect of machining and post-treatments on surface residual stress. International Journal of Advancements in Mechanical and Aeronautical Engineering– IJAMAE Volume 2: Issue 2
24. Bursi O.S, D'Incau M, Zanon G, Raso S & Scardi P. 2017. Laser and mechanical cutting effects on the cut-edge properties of steel S355N. Journal of Constructional Steel Research June 2017, Vol.133, pp.181-191
25. Pessoa D.F, Herwig P, Wetzig A & Zimmermann M. 2017. Influence of surface condition due to laser beam cutting on the fatigue behavior of metastable austenitic stainless steel AISI 304. Engineering Fracture Mechanics. Volume 185, November 2017. pp. 14.
26. Salo J. 2016. Fatigue strength of welded joints in super-duplex stainless steel. [Master's Thesis] pp. 93.
27. Mattila M. 2016. Investigation of the fatigue performance of welded duplex stainless steel. [Master's Thesis] pp. 105.
28. Murakami Y. Metal fatigue: effects of small defects and nonmetallic inclusions. 1st ed. Netherlands: Elsevier Science Ltd.; 2002.
29. Kanyilmaz A. 2019.The problematic nature of steel hollow section joint fabrication, and a remedy using laser cutting technology: A review of research, applications, opportunities. Engineering Structures. Volume 183, 15 March 2019, Pages 1027-1048

Appendix

Table A1. Fatigue test results.

Material	Cutting method	Edge condition	Stress ratio [-]	Nominal stress range [MPa]	Fatigue life [cycles]
S690QL	CO_2 laser	As-cut	0.1	436	346812
S690QL	CO_2 laser	As-cut	0.1	523	138998
S690QL	CO_2 laser	As-cut	0.1	363	580883
S690QL	CO_2 laser	As-cut	0.1	331	781237
S690QL	CO_2 laser	As-cut	0.1	290	2000000
S690QL	CO_2 laser	As-cut	0.5	331	2000000
S690QL	CO_2 laser	As-cut	0.4	397	379140
S690QL	CO_2 laser	As-cut	0.4	363	364232
S690QL	CO_2 laser	As-cut	0.4	347	688636
S690QL	CO_2 laser	As-cut	0.4	397	277650
S690QL	Fiber laser N_2	As-cut	0.1	436	118241
S690QL	Fiber laser N_2	As-cut	0.1	407	154720
S690QL	Fiber laser N_2	As-cut	0.1	334	350450
S690QL	Fiber laser N_2	As-cut	0.1	305	340198
S690QL	Fiber laser N_2	As-cut	0.1	261	495111
S690QL	Fiber laser N_2	As-cut	0.4	397	176831
S690QL	Fiber laser N_2	As-cut	0.4	323	208983
S690QL	Fiber laser N_2	As-cut	0.4	290	318504
S690QL	Fiber laser N_2	As-cut	0.4	210	599176
S690QL	Fiber laser N_2	Burr ground	0.1	436	193234
S690QL	Plasma	As-cut	0.1	581	98593
S690QL	Plasma	As-cut	0.1	484	150823
S690QL	Plasma	As-cut	0.1	371	383292
S690QL	Plasma	As-cut	0.1	332	402428
S690QL	Plasma	As-cut	0.1	290	1523830
S690QL	Plasma	As-cut	0.1	319	354604
S690QL	Plasma	As-cut	0.4	397	220777
S690QL	Plasma	As-cut	0.4	307	444627
S690QL	Plasma	As-cut	0.4	290	554439
S690QL	Plasma	As-cut	0.4	272	620505
S690QL	Plasma	Burr ground	0.1	581	104807
S690QL	Machined	As-cut	0.4	410	629379
S1100	Fiber laser N_2	As-cut	0.1	675	29195
S1100	Fiber laser N_2	As-cut	0.1	523	94321
S1100	Fiber laser N_2	As-cut	0.1	402	346379
S1100	Fiber laser N_2	As-cut	0.1	348	2000000
S1100	Fiber laser N_2	As-cut	0.1	380	404035
S1100	Fiber laser N_2	As-cut	0.1	364	297340
S1100	Fiber laser N_2	Burr ground	0.1	523	232728
S1100	Fiber laser N_2	As-cut	0.5	477	88481
S1100	Fiber laser N_2	As-cut	0.5	374	216890
S1100	Fiber laser N_2	As-cut	0.5	327	304158
S1100	Fiber laser N_2	As-cut	0.5	363	328591
S1100	Fiber laser N_2	As-cut	0.5	339	2000000
S1100	Fiber laser N_2	As-cut	0.5	424	138443
S1100	Fiber laser O_2	As-cut	0.1	698	63599